Evaluation of density functional theory for a large and diverse set of organic and inorganic equilibrium structures

Amir Karton* and Peter R. Spackman

School of Molecular Sciences, The University of Western Australia, Perth, WA 6009, Australia.

ABSTRACT: Density functional theory (DFT) has been extensively benchmarked for energetic properties; however, less attention has been given to equilibrium structures and the effect of using a certain DFT geometry on subsequent energetic properties. We evaluate the performance of 52 contemporary DFT methods for obtaining the structures of 122 species in the W4-11-GEOM database. This dataset includes a total of 246 unique bonds: 117 H–X, 65 X–Y, 49 X=Y, and 15 X≡Y bonds (where X and Y are first- and second-row atoms) and 133 key bond angles: 96 X-Y-H, 22 X-Y-Z, and 15 H-X-H angles. The reference geometries are optimized at the CCSD(T)/jul-cc-pV(*n*+d)Z level of theory (*n* = 5, 6). The performance of DFT is evaluated in conjunction with the Def2-*n*ZVPP (*n* = T, Q), cc-pV(T+d)Z, and jul-cc-pV(T+d)Z basis sets. The root-mean-square deviations (RMSDs) over the bond distances of the best performing functionals from each rung of Jacob's Ladder are 0.0086 (SOGGA11), 0.0088 (τ-HCTH), 0.0058 (X3LYP), 0.0054 (TPSSh), and 0.0032 (DSD-PBEP86) Å. We evaluate the effect of the choice of the DFT geometry on subsequent molecular energies calculated with W1-F12 theory. Geometries obtained with GGA and MGGA methods result in large RMSDs in the subsequent W1-F12 energies; however, six hybrid GGA functionals (B3LYP, B3P86, mPW3PBE, B3PW91, mPW1LYP, and X3LYP) result in an excellent performance with RMSDs between 0.25–0.30 kJ mol^{-1} relative to the CCSD(T)/CBS reference geometries. The B2GP-PLYP and mPW2-PLYP DHDFT methods result in near-CCSD(T) accuracy with RMSDs of 0.11 and 0.10 kJ mol^{-1}, respectively.

Keywords: geometry optimization • molecular structures • DFT • DHDFT • CCSD(T)

Cite as:
A. Karton, P. R. Spackman. Evaluation of density functional theory for a large and diverse set of organic and inorganic equilibrium structures. *J. Comput. Chem.* 42, 1590–1601 (2021). https://doi.org/10.1002/jcc.26698

*E-Mail: amir.karton@uwa.edu.au

1. Introduction

The concept of a molecular structure is fundamental to our understanding of chemistry and obtaining equilibrium molecular structures is the first step in most computational chemistry studies. A typical geometry optimization of a complex chemical system requires a large number of single-point energy calculations and, in addition, most efficient geometry optimization algorithms rely on at least the first derivatives of the energy.[1,2,3] Thus, electronic structure methods used for geometry optimizations of medium-sized (or large) molecular systems need to be computationally efficient and robust. Over the past three decades, density functional theory (DFT) has become the dominant electronic structure method for obtaining molecular structures due to its attractive accuracy-to-computational cost ratio. For example, the popular B3LYP exchange correlation (XC) functional[4] is used as the method of choice for calculating molecular structures in many composite ab initio methods that are approximating the CCSD(T) energy (coupled-cluster with single, double, and quasiperturbative triple excitations) near the one-particle basis set limit, e.g., W*n*[5] and W*n*-F12 (*n* = 1, 2),[6,7] ccCA,[8] G4,[9] G4(MP2),[9] and CBS-QB3.[10] Other CCSD(T) composite methods have adopted other DFT functionals for the geometry optimizations, e.g., BMK[11] in the G4(MP2)-6X method.[12] A fundamental limitation of the DFT formalism is the lack of a universal XC DFT functional,[13,14] which has led to a proliferation in the number of developed DFT methods over the past couple of decades.[15] Therefore, the validation of DFT functionals has become an important step before using DFT for calculating a given chemical property.

DFT has been extensively benchmarked for a wide range of thermochemical properties (e.g., reaction, isomerization, and conformational energies), with hundreds of benchmark studies have been published in this area over the past two decades. For an overview see, for example, refs. 16,17,18,19,20. However, less attention has been given to benchmarking equilibrium structures of main-group compounds and the effect of using a certain DFT

geometry on subsequent thermochemical properties. Adamo and co-workers,[21] benchmarked a wide range of XC functionals for the CH, CO, and CC bonds of closed-shell organic molecules in the CCse21 and B3se47 databases of semi-experimental equilibrium structures.[22,23] More recently,[24] Morgante and Peverati presented an interesting benchmark study focusing on long C–C bond lengths where the reference bond distances were taken from the experimental crystal structures. The datasets used in these benchmark studies, however, focus almost exclusively on bonds between first-row atoms (and hydrogen). In addition, the conversion of experimental bond distances to electronic bond distances (r_e) on the Born–Oppenheimer (BO) potential energy surface (PES) involves back-correcting for effects that are not explicitly included in the DFT geometry optimizations (such as effects of different isotopologues and vibrational contributions),[1,2,22,25] which by necessity increases the uncertainty of the reference values.

In the present work, we assess the performance of DFT methods across the rungs of Jacob's Ladder for the molecular structures in the W4-11-GEOM database.[26,27] The reference geometries have been optimized on the electronic PES at the CCSD(T)/CBS level of theory. The W4-11-GEOM database includes 122 species, which cover a broad spectrum of bonding situations with a range of single and multiple bonds that involve varying degrees of covalent and ionic characters. As such this database constitutes an excellent benchmark set for evaluating the performance of DFT for a wide and diverse range of equilibrium structures.

2. Computational Methods

We use the CCSD(T)/CBS (i.e., coupled cluster with single, double, and quasiperturbative triple excitations close to the complete basis set limit) reference structures in the W4-11-GEOM database to evaluate the performance of a wide range of DFT methods. The DFT XC functionals considered in the present study (ordered by their rung on Jacob's Ladder) are given in Table 1.

Table 1. DFT exchange-correlation functionals considered in the present work.

Type[a]	Functionals
GGA (8)	BLYP,[28,29] B97-D,[30] HCTH407,[31] PBE,[32] BP86,[28,33] BPW91,[29,34] SOGGA11,[35] N12[36]
MGGA (7)	M06-L,[37] TPSS,[38] τ-HCTH,[39] VSXC,[40] M11-L,[41] MN12-L,[42] MN15-L[43]
HGGA (17)	BH&HLYP,[44] B3LYP,[28,45,46] B3P86,[45,33] B3PW91,[45,34] PBE0,[47] B97-1,[48] X3LYP,[49] SOGGA11-X,[50] APF,[51] mPW1PBE,[32,52] mPW1PW91,[34,52] mPW3PBE,[32,52] mPW1LYP,[28,52] ωB97,[53] ωB97X,[53] N12-SX,[b,54] CAM-B3LYP[b,55]
HMGGA (14)	M05,[56] M05-2X,[57] M06,[58] M06-2X,[58] M06-HF,[58] M08-HX,[59] MN15,[43] BMK,[60] B1B95,[61,28] TPSSh,[62] τ-HCTHh,[39] PW6B95,[63] MN12-SX,[b,54] M11[b,64]
DH (6)	B2-PLYP,[65] mPW2-PLYP,[66] B2GP-PLYP,[67] DSD-PBEP86,[68,69] PBE0-DH,[70] PBEQI-DH[71]

[a]GGA = generalized gradient approximation, MGGA = meta-GGA, HGGA = hybrid-GGA, HMGGA = hybrid-meta-GGA, DH = double hybrid, MP = Møller–Plesset perturbation theory, Ab Initio = composite ab initio methods. [b]Range separated XC functional.

All the standard DFT and DHDFT geometry optimizations were carried out utilizing the Karlsruhe-type Def2-*n*ZVPP (n = T, Q) basis sets,[72] and the correlation-consistent cc-pV(T+d)Z and jul-cc-pV(T+d)Z basis sets.[73,74,75,76] These calculations were performed using a large pruned (99,590) integration grid and all single point energies were converged to 10^{-8} a.u. We also note that all DFT geometry optimizations started from the optimized CCSD(T)/CBS reference geometries. All the CCSD(T) calculations involved in W1-F12 theory were

calculated using Molpro 2016,[77,78] while all the other calculations (DFT, DHDFT, MP2, and lower-level composite procedures) were performed using the Gaussian 16 program suites.[79]

All DFT and DHDFT geometry optimizations were followed by harmonic vibrational frequency calculations at the same level of theory to confirm that the stationary points are equilibrium structures, i.e., they have only real frequencies. It should be noted, however, that well-known pathological cases, most notably oxirene,[80,81,82] were verified to be first-order saddle points characterized by one imaginary frequency at some levels of theory.

3. Results and Discussion

Overview of reference geometries and bond distances in the W4-11-GEOM database. The reference geometries in the W4-11-GEOM database were optimized at the CCSD(T)/jul-cc-pV(6+d)Z level of theory, except for a small subset of larger molecules with low spatial symmetries for which the reference geometries were optimized at the CCSD(T)/jul-cc-pV(5+d)Z level of theory (for further details see Table S1 of the Supporting Information). The W4-11-GEOM dataset includes 122 molecules (85 closed shell, 21 radical, 9 singlet carbene, and 7 triplet species). In terms of elemental composition, the dataset includes 88 first-row species (containing H and B–F), 17 second-row species (containing H and Al–Cl), and 17 mixed first- and second-row species (containing H, B–F, and Al–Cl atoms). Table 2 gives an overview of the types of bonds in the W4-11-GEOM dataset. Overall, the database includes 246 symmetry-unique bonds. Namely, 117 single bonds involving hydrogen (H–X), 65 single bonds between non-hydrogen atoms (X–Y), 49 double bonds (X=Y), and 15 triple bonds (X≡Y), where X and Y are non-hydrogen atoms from the first and second rows of the Periodic Table. For the complete list of bonds in the W4-11-GEOM dataset see Table S1 of the Supporting Information. For the purpose of the discussion below, each of the H–X, X–Y, X=Y,

and X≡Y bonds can be further divided into carbon containing bonds (referred to as the organic subset) and bonds without carbon (referred to as the inorganic subset).

Table 2. Overview of the 246 unique bonds in the W4-11-GEOM database.[a,b]

Bond type	Organic[c]	Inorganic[d]	Overall	Comment
H–X	65	52	117	X = B–F, Al–Cl
X–Y	37	28	65	X, Y = B–F, Al–Cl
X=Y	29	20	49	X, Y = C, N, O, Si, S, Cl
X≡Y	12	3	15	X, Y = B, C, N, P
All	143	103	246	X = H, B–F, Al–Cl

[a]For the complete list of bonds, see Table S1 of the Supporting Information. [b]Unique bonds are not equivalent by symmetry, for example CH_3Cl has two unique bonds (C–H and C–Cl). [c]X and/or Y is a carbon. [d]Not containing carbon.

Overall performance for the 246 bonds in the W4-11-GEOM database. Table 3 gives an overview of the performance of DFT and DHDFT procedures for the 246 symmetry-unique single, double, and triple bonds in the W4-11-GEOM database (for the performance for the organic and inorganic subsets see Table S2 of the Supporting Information). The GGA methods result in relatively poor performance with RMSDs ranging between 0.009 (HCTH407) and 0.018 (BLYP) Å. Inclusion of the kinetic energy density does not seem to improve the performance, with the MGGA methods resulting in RMSDs ranging between 0.008 (M06-L) and 0.022 (M11-L) Å. Notably, the older generation MGGA (without range separation) performs better than the dual-range M11-L functional. As expected, inclusion of exact exchange in the HGGA functionals results in improvements in performance over the GGA functionals. In particular, the best HGGA methods (B97-1, mPW1LYP, B3LYP, and X3LYP) result in an RMSD of 0.006 Å compared to an RMSD of 0.009 Å obtained for the best GGA (HCTH407). Inclusion of both exact exchange and the kinetic energy density results in an additional small improvement in performance. Namely, the best HMGGA method (TPSSh) results in an RMSD of 0.005 Å. The DHDFT functionals result in excellent performance with RMSDs ranging between 0.003 (DSD-PBEP86) and 0.004 (B2GP-PLYP) kJ mol^{-1}, with the

exception of the parameter free PBE0-DH and PBEQI-DH procedures, which attain RMSDs > 0.01 Å.

Table 3. Overview of the performance of DFT procedures in conjunction with the Def2-TZVPP basis set for the 246 bonds in the W4-11-GEOM database and subsets of single, double, and triple bonds (RMSDs are given in Å).[a,b]

		All (246)	X–H (117)	X–Y (65)	X=Y (49)	X≡Y (15)
GGA	BLYP	0.0179	0.0110	0.0288	0.0137	0.0092
	BP86	0.0137	0.0128	0.0178	0.0103	0.0079
	B97-D	0.0126	0.0091	0.0172	0.0075	0.0218
	PBE	0.0124	0.0125	0.0149	0.0095	0.0066
	BPW91	0.0123	0.0110	0.0168	0.0094	0.0057
	N12	0.0100	0.0063	0.0133	0.0121	0.0097
	HCTH407	0.0094	0.0064	0.0112	0.0071	0.0207
	SOGGA11	0.0086	0.0079	0.0109	0.0077	0.0043
MGGA	M11-L	0.0218	0.0103	0.0329	0.0250	0.0156
	MN12-L	0.0113	0.0051	0.0159	0.0136	0.0141
	TPSS	0.0106	0.0075	0.0163	0.0084	0.0043
	MN15-L	0.0101	0.0129	0.0086	0.0034	0.0046
	VSXC	0.0095	0.0044	0.0135	0.0052	0.0213
	τ-HCTH	0.0088	0.0059	0.0099	0.0068	0.0207
	M06-L	0.0084	0.0038	0.0100	0.0079	0.0200
HGGA	BH&HLYP	0.0155	0.0081	0.0193	0.0198	0.0231
	SOGGA11-X	0.0091	0.0025	0.0139	0.0104	0.0112
	PBE0	0.0084	0.0033	0.0125	0.0098	0.0099
	mPW1PBE	0.0084	0.0026	0.0122	0.0102	0.0105
	mPW1PW91	0.0082	0.0022	0.0118	0.0104	0.0110
	APF	0.0076	0.0033	0.0108	0.0091	0.0093
	B3P86	0.0071	0.0024	0.0097	0.0091	0.0095
	mPW3PBE	0.0069	0.0036	0.0093	0.0084	0.0084
	B3PW91	0.0065	0.0033	0.0086	0.0082	0.0085
	B97-1	0.0060	0.0038	0.0090	0.0054	0.0063
	mPW1LYP	0.0060	0.0018	0.0070	0.0086	0.0105
	B3LYP	0.0059	0.0027	0.0077	0.0075	0.0083
	X3LYP	0.0058	0.0024	0.0070	0.0080	0.0092
HMGGA	M06-HF	0.0150	0.0044	0.0203	0.0186	0.0245
	M08-HX	0.0106	0.0042	0.0143	0.0133	0.0154
	BMK	0.0104	0.0032	0.0165	0.0105	0.0126
	M05-2X	0.0102	0.0034	0.0140	0.0129	0.0150
	MN15	0.0100	0.0040	0.0157	0.0092	0.0133
	M06	0.0100	0.0032	0.0152	0.0117	0.0107
	M05	0.0098	0.0031	0.0168	0.0090	0.0053
	M06-2X	0.0097	0.0017	0.0139	0.0118	0.0149
	B1B95	0.0091	0.0020	0.0131	0.0117	0.0121
	PW6B95	0.0088	0.0033	0.0113	0.0119	0.0131

	τ-HCTHh	0.0076	0.0044	0.0082	0.0055	0.0201
	TPSSh	0.0054	0.0040	0.0074	0.0053	0.0047
RS	N12-SX	0.0108	0.0041	0.0153	0.0134	0.0139
	M11	0.0106	0.0044	0.0145	0.0128	0.0159
	MN12-SX	0.0106	0.0063	0.0143	0.0119	0.0135
	ωB97	0.0099	0.0027	0.0153	0.0098	0.0147
	ωB97-X	0.0095	0.0018	0.0137	0.0111	0.0149
	CAM-B3LYP	0.0086	0.0014	0.0103	0.0121	0.0159
DH	PBE0-DH	0.0115	0.0032	0.0181	0.0126	0.0122
	PBEQI-DH	0.0106	0.0043	0.0169	0.0107	0.0099
	MP2	0.0081	0.0030	0.0053	0.0124	0.0197
	B2GP-PLYP	0.0043	0.0030	0.0051	0.0054	0.0050
	mPW2-PLYP	0.0043	0.0026	0.0050	0.0058	0.0052
	B2-PLYP	0.0039	0.0016	0.0054	0.0053	0.0029
	DSD-PBEP86	0.0032	0.0010	0.0037	0.0044	0.0059

[a]GGA = generalized gradient approximation, HGGA = hybrid-GGA, MGGA = meta-GGA, HMGGA = hybrid-meta-GGA, RS = range-separated, DH = double hybrid. [b]The reference CCSD(T)/CBS bond distances are given in Table S3.

For the sake of completeness, we also examine the effect of empirical dispersion corrections on the performance of some of the of DFT functionals for the bond distances in the W4-GEOM-11 database. It should be stressed, however, that since the largest systems in this database are small monomers such as propane, ethanol, and acetic acid, long range intramolecular interactions are not expected to play a significant role in their structure determination. Table S4 of the Supporting Information gathers the differences in RMSDs over the 246 bond distances in the W4-11-GEOM database between the dispersion-corrected (using the D3BJ dispersion correction)[83,84,85,86] and uncorrected DFT functionals. As expected, across all rungs of Jacob's Ladder, inclusion of the D3BJ correction has no visible effect on the performance of the DFT functionals. The largest change in the RMSD is observed for the BLYP functional, where the inclusion of the D3BJ correction reduces the RMSD by merely 0.0001 Å. The effects on the RMSDs for the other functionals are about an order of magnitude smaller than that (see Table S4). These results demonstrate that the geometries in the W4-11-GEOM database are generally free from significant dispersion effects. Thus, this database

provides an evaluation of the performance of the underlying DFT functional without confounding dispersion effects.

Overview of performance for X–H bonds. Table 3 gives an overview of the performance of the DFT and DHDFT procedures for the 117 hydride bonds (X–H) in the W4-11-GEOM database. Let us start with examining the performance for the entire set of hydride bonds. Over the entire set of hydride bonds GGAs show relatively poor performance, excepting HCTH407 (0.0064) and N12 (0.0063), with RMSDs ranging between 0.008–0.013 Å. Two of the MGGAs (VSXC and M06-L) show much better performance with RMSDs of 0.004 Å. Nearly all HGGA and HMGGA functionals demonstrate much better performance with RMSDs ranging between 0.002–0.004 Å. Specifically, the best performing methods attain RMSDs of 0.0018 (mPW1LYP) and 0.0017 (M06-2X) Å. The DHDFT methods result in RMSDs ranging between 0.001–0.004 Å, where the best performing methods are DSD-PBEP86 and B2-PLYP with RMSDs of 0.0010 and 0.0016 Å, respectively. Overall, with the main exception of the GGA functionals, nearly all of the MGGA, HGGA, HMGGA, RS, and DH methods attain RMSDs < 0.006 Å.

Table S5 gives an overview of the performance for the subsets of organic (C–H) and inorganic (X–H, X = B, N–Cl) bonds. Most functionals exhibit slightly better performance for the organic C–H bonds over the inorganic X–H bonds. However, the differences in performance are relatively small. In most cases the ratio between the two RMSDs ($RMSD_{X–H}/RMSD_{C–H}$) is below 1.5.

Overview of performance for single bonds between heavy atoms. Moving to the set of 65 single X–Y bonds (X, Y = B–F and Al–Cl), inspection of the results in Table 3 shows that performance for the X–Y bonds is significantly worse than for X–H bonds. Most of the DFT methods from rungs 2–4 of Jacob's Ladder result in RMSDs ranging between 0.01–0.02 Å.

The best performing functionals from each rung of Jacob's Ladder are the GGAs SOGGA11 (0.0109) and HCTH407 (0.0112); MGGAs MN15-L (0.0086) and τ-HCTH (0.0099); HGGAs X3LYP (0.0070) and mPW1LYP (0.0070); and HMGGAs TPSSh (0.0074) and τ-HCTH (0.0082 Å). DHDFT methods show consistently better performance over conventional DFT procedures. The B2-PLYP, mPW2-PLYP, B2GP-PLYP show very similar performance with RMSDs ranging between 0.0050–0.0054 Å. MP2 essentially attains the same performance with an RMSD of 0.0053 Å. The spin-component-scaled DSD-PBEP86-D3BJ method results in exceptionally good performance with an overall RMSD of merely 0.0037 Å. However, the parameter-free PBE0-DH and PBEQI-DH procedures result in poor performance with RMSDs of 0.017–0.018 Å.

It is instructive to compare the performance for organic single bonds (C–X, X = C, N, O, F, Cl) with the inorganic single bonds (B–F, N–N, N–O, N–Cl, O–O, O–F, O–Cl, F–F, F–Cl, F–Si, Al–F, Al–Cl, Si–Si, P–P, S–S, Cl–Cl). Inspection of Table S6 of the Supporting Information reveals that the performance is systematically and significantly worse for the subset of inorganic bonds. This may be attributed to stronger multireference and polar nature of the inorganic bonds. This is particularly pronounced for four of the HMGGA methods from the Minnesota family (M05-2X, M06-2X, M06-HF, and M08-HX) which show substantially deteriorated performance for the inorganic bonds with RMSDs that are 3–4 times larger than of the organic bonds. Overall, the DSD-PBEP86 DHDFT method shows exceptionally good performance for both organic and inorganic bonds with RMSDs of 0.0020 and 0.0052 Å, respectively.

Overview of performance for double X=Y bonds. Table 3 gives an overview of the performance for the 49 double bonds in the W4-11-GEOM database. The best performers over these bonds are (RMSDs given in parentheses): the GGAs B97-D (0.0075) and HCTH407

(0.0071); the MGGAs VSXC (0.0052) and MN15-L (0.0034); the HGGA B97-1 (0.0054); the HMGGAs τ-HCTHh (0.0055) and TPSSh (0.0053); the DHDFT methods B2-PLYP (0.0053) and DSD-PBEP86 (0.0044 Å). Thus, when considering the best performing functionals, there is little overall improvement when going from MGGAs to HGGAs, HMGGAs, and even DHDFT methods. It should be pointed out, however, that compared to DHDFT, MP2 shows significantly deteriorated performance for double bonds with an overall RMSD of 0.0124 Å. We also note that the MGGAs, HGGAs, HMGGAs, and DHDFT methods show similar performance for the organic C=X and inorganic X=Y bonds (Table S7 of the Supporting Information), however, the GGAs tend to result in larger errors for the latter bonds.

Overview of performance for triple X≡Y bonds. The W4-11-GEOM database includes 15 triple bonds, 12 of which involve carbon. Overview of the performance of DFT and DHDFT procedures for the triple bonds is given in the last column of Table 3. Most of the DFT methods from rungs 2–4 of Jacob's Ladder result in RMSDs ranging between 0.008–0.027 Å. The best performing functionals from each category are the GGAs SOGGA11 (0.0043) and BPW91 (0.0057); MGGAs TPSS (0.0043) and MN15-L (0.0046); HGGAs B97-1 (0.0063) and B3LYP (0.0083); HMGGAs TPSSh (0.0047) and M05 (0.0053 Å). Again, DHDFT methods show consistently better performance over conventional DFT procedures. Of the DHDFT methods, B2-PLYP shows the best performance with an RMSD of 0.0029 Å. The B2GP-PLYP and mPW2-PLYP methods tie in second place with RMSDs of 0.0050 and 0.0052 Å, respectively. Similar to the performance for double bonds, MP2 shows significantly deteriorated performance relative to DHDFT for the triple bonds with an overall RMSD of 0.0197 Å.

Overview of performance for bond angles. It is of interest to also examine the performance of the DFT and DHDFT methods for the equilibrium bond angles in the W4-11-GEOM

database. For this purpose, we selected 133 key bond angles, specifically: 96 X-Y-H, 22 X-Y-Z, and 15 H-X-H angles (where X, Y, and Z are non-hydrogen atoms). For the complete list of angles along with the CCSD(T)/CBS reference values see Table S8 of the Supporting Information. Table 4 gives an overview of the performance of the DFT and DHDFT procedures for these 133 bond angles. Inspection of the error statistics in Table 4 reveals two key findings: (i) on average, most DFT methods tend to overestimate the bond angles, as evident from positive mean-signed deviations (MSDs), and (ii) nearly all of the conventional DFT methods attain RMSDs ranging between 0.5–1.0°. The GGA, MGGA, and range-separated hybrid methods show relatively poor performance with RMSDs ranging between 0.50° (TPSS) and 1.06° (M11). The best performing HGGA and HMGGA methods attain RMSDs below 0.5°, namely: 0.49° (τ-HCTHh), 0.44° (B97-1 and SOGGA11-X), and 0.41° (TPSSh). With the exception of PBE0-DH for which we obtain an RMSD of 0.51°, all the DHDFT methods result in excellent performance with RMSDs ranging between 0.25° (DSD-PBEP86) and 0.40° (mPW2-PLYP and PBEQI-DH). For comparison MP2 attains a substantially larger RMSD of 0.66°. Of particular note is the exceptionally good performance of the DSD-PBEP86 method with RMSD and MAD of 0.25° and 0.16°, respectively. It is also noteworthy that the largest deviation for DSD-PBEP86 is merely 1.24°, for comparison the largest deviation for MP2 is 5.1° (see Supporting Information for further details).

Table 4. Overview of the performance of DFT procedures in conjunction with the Def2-TZVPP basis set for the 133 bond angles in the W4-11-GEOM database (error statistics are given in °).[a,b,c]

		RMSD	MAD	MSD
GGA	N12	0.94	0.63	0.42
	SOGGA11	0.88	0.63	0.32
	BLYP	0.69	0.51	0.13
	HCTH407	0.67	0.52	0.24
	BPW91	0.59	0.45	0.14
	PBE	0.58	0.44	0.14
	BP86	0.58	0.44	0.12

	B97-D	0.57	0.42	0.13
MGGA	M11-L	0.79	0.65	0.13
	VSXC	0.73	0.56	0.12
	MN12-L	0.70	0.53	0.28
	τ-HCTH	0.63	0.49	0.22
	M06-L	0.62	0.52	0.21
	MN15-L	0.56	0.41	0.00
	TPSS	0.50	0.38	0.05
HGGA	BH&HLYP	0.80	0.55	0.43
	X3LYP	0.62	0.46	0.30
	B3LYP	0.62	0.45	0.29
	mPW1LYP	0.60	0.45	0.30
	B3P86	0.56	0.42	0.29
	mPW3PBE	0.55	0.42	0.28
	B3PW91	0.55	0.42	0.28
	mPW1PW91	0.54	0.42	0.29
	APF	0.54	0.41	0.28
	mPW1PBE	0.53	0.41	0.29
	PBE0	0.53	0.41	0.29
	B97-1	0.44	0.34	0.19
	SOGGA11-X	0.44	0.33	0.21
HMGGA	M06-HF	1.17	0.84	0.40
	MN15	0.87	0.55	0.43
	M06	0.79	0.60	0.40
	M05	0.77	0.58	0.36
	M08-HX	0.76	0.48	0.39
	BMK	0.63	0.39	0.29
	M05-2X	0.61	0.38	0.28
	M06-2X	0.58	0.37	0.29
	B1B95	0.56	0.41	0.29
	PW6B95	0.55	0.39	0.29
	τ-HCTHh	0.49	0.37	0.20
	TPSSh	0.41	0.30	0.13
RS	M11	1.06	0.61	0.51
	N12-SX	1.04	0.66	0.53
	CAM-B3LYP	0.71	0.48	0.37
	MN12-SX	0.61	0.47	0.29
	ωB97-X	0.54	0.37	0.29
	ωB97	0.54	0.35	0.26
DH	MP2	0.66	0.26	0.04
	PBE0-DH	0.51	0.38	0.28
	PBEQI-DH	0.40	0.29	0.22
	mPW2-PLYP	0.40	0.28	0.19
	B2-PLYP	0.38	0.26	0.15
	B2GP-PLYP	0.37	0.26	0.15
	DSD-PBEP86	0.25	0.16	0.09

[a]GGA = generalized gradient approximation, HGGA = hybrid-GGA, MGGA = meta-GGA, HMGGA = hybrid-meta-GGA, RS = range-separated, DH = double hybrid. [b]The reference CCSD(T)/CBS bond angles are given in Table S8. [c]RMSD = root-mean-square deviation, MAD = mean-absolute deviation, MSD = mean-signed deviation.

Optimal percentage of exact Hartree–Fock exchange. It is instructive to examine the relationship between the percentage of exact HF exchange in a given functional and its performance. Figure 1 plots the RMSDs over the 246 bonds in the W4-11-GEOM database and percentage of exact Hartree–Fock exchange for the HGGAs. Here it is evident that functionals with 20–25% of exact-exchange (EXX) admixture show the best performance. For example, B3LYP (20% EXX), B97-1 (21% EXX), and mPW1LYP (25% EXX) attain the lowest RMSDs of 0.006 Å. To examine this further, we chose two GGAs (BLYP and PBE) and two meta GGAs (τ-HCTH and TPSS) and scanned the percentage of exact HF exchange by adding exact exchange to the pure functionals. The MSDs and RMSDs over the 246 bonds in the W4-11-GEOM database are depicted in Figure 2. The MSDs vary linearly with the percentage of EXX for all four functionals, where no EXX admixture leads to positive MSDs of up to 0.01 Å and 100% of EXX admixture results in large negative MSDs of up to –0.03 Å. The MSD curve crosses the x-axis at 2.3% (τ-HCTH) and 24.1% (BLYP), thus there is a substantial variation in the optimal percentage of EXX admixture between the four functionals. Figure 2 also shows that at the EXX percentage for which the MSDs are zero, all the functionals result in small RMSDs. In particular, the RMSDs are around the minimum are: 0.0041 (TPSS), 0.0057 (PBE), 0.0060 (BLYP), and 0.0073 (τ-HCTH) Å (Figure 2). For comparison, the RMSDs are obtained for the original semi-local functionals are significantly higher, namely: 0.0106 (TPSS), 0.0124 (PBE), 0.0179 (BLYP), and 0.0088 (τ-HCTH) Å (Table 3). The one exception being τ-HCTH which exhibits a very shallow minimum around 13.6%, and all values between 2–20% yield roughly comparable performance.

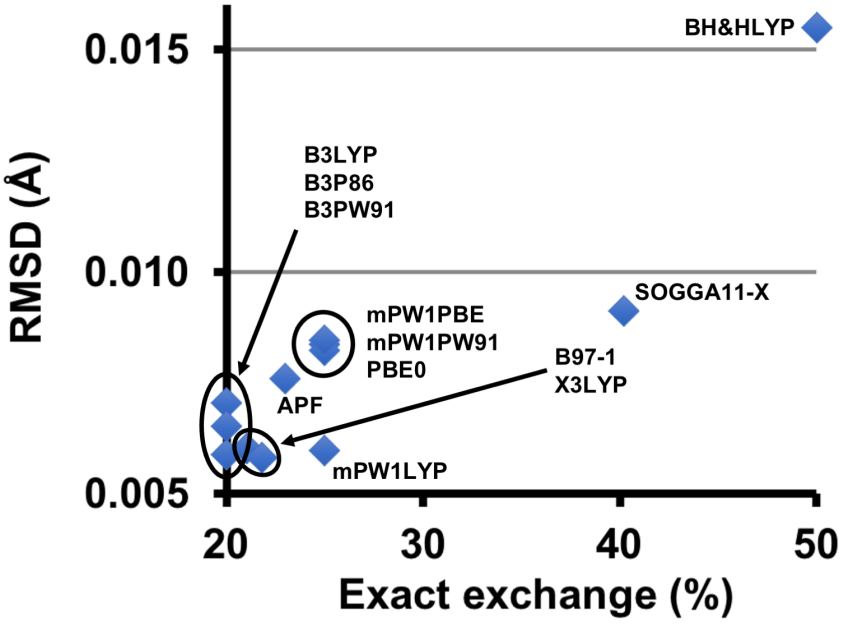

Figure 1. Relationship between the RMSDs over the 246 unique bonds in the W4-11-GEOM database and the percentage of exact exchange mixing coefficient for the HGGA functionals. The RMSDs are taken from Table 3.

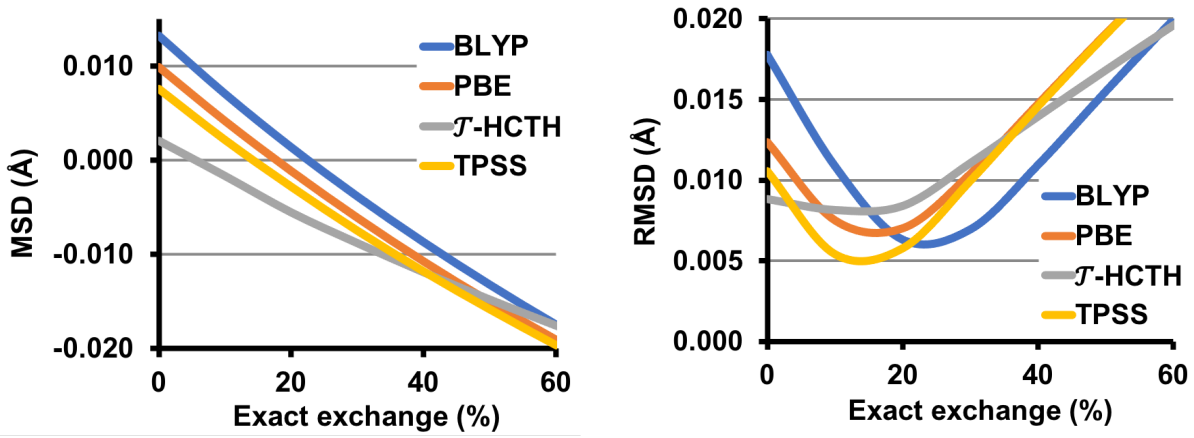

Figure 2. Dependence of the mean-signed deviation (MSD) and root-mean-square deviations (RMSDs) over the 246 unique bonds in the W4-11-GEOM database on the exact exchange mixing coefficient for two GGA (BLYP and PBE) and two meta-GGA (t-HCTH and TPSS) functionals.

Basis set dependency of the DFT and DHDFT bond distances. Table S9 of the Supporting Information gathers the differences in RMSD between the geometries optimized with the Def2-TZVPP and Def2-QZVPP basis sets for the 246 bonds in the W4-11-GEOM database (ΔRMSD = RMSD(Def2-TZVPP) – RMSD(Def2-QZVPP). A positive ΔRMSD value indicates an improvement in performance when moving from the Def2-TZVPP to the Def2-QZVPP basis set. Inspection of Table S9 reveals two interesting trends. (i) Two thirds of the ΔRMSD values are negative, i.e., most functionals exhibit an overall slight deterioration in performance with the larger basis set. (ii) With the exception of 11 DFT methods and 4 DHDFT methods, all the ΔRMSD values are below 0.0005 Å (in absolute value), that is the basis set dependence is at this point is very small. These results indicate that, at least for the relatively small systems considered in the present work, the Def2-TZVPP bond distances are sufficiently close to the Def2-QZVPP bond distances such that the use of the larger basis does not seem to be warranted. Overall, only three methods exhibit a significant basis set dependence with ΔRMSD > 0.001 Å, namely (ΔRMSDs are given in parentheses): M06-HF (–0.0024), SOGGA11 (–0.0015), and PBEQI-DH (–0.0011 Å). It has been previously noted that the M06-HF and SOGGA11 functionals exhibit a somewhat erratic basis set dependence.[87,88]

It is also of interest to examine the performance of the DFT and DHDFT methods in conjunction with the correlation-consistent cc-pV(T+d)Z and jul-cc-pV(T+d)Z basis sets. This allows a comparison between the Karlsruhe-type and correlation-consistent basis sets, as well as an examination of the effect of diffuse functions on the DFT geometries. Table S10 of the Supporting Information gives the RMSDs over the 246 bonds in the W4-11-GEOM database for the correlation-consistent basis sets. Comparison between the RMSDs for the Def2-TZVPP and cc-pV(T+d)Z basis sets reveals that, with the main exception of the GGA and MGGA methods, the cc-pV(T+d)Z basis set exhibits somewhat better performance than Def2-TZVPP. However, in most cases the differences between the RMSDs for the two basis sets are small

and do not exceed 0.0004 Å. For the Minnesota functionals the RMSDs for the cc-pV(T+d)Z basis set are smaller than those for the Def2-TZVPP basis set by somewhat larger amounts, namely: 0.0005 (SOGGA11-X, M06-HF, M06-2X, M05-2X), 0.0006 (M11-L), and 0.0007 (M08-HX, M11) Å. Comparison of the RMSDs for the cc-pV(T+d)Z and jul-cc-pV(T+d)Z basis sets (Table S10) reveals that addition of diffuse functions has a relatively minor effect on performance. With two exceptions, the RMSDs for the two basis sets differ by up to 0.0004 Å. Interestingly, for two Minnesota functionals addition of the diffuse functions results in deterioration in performance by 0.0005 (M11-L) and 0.0007 (SOGGA11) Å.

Energetic consequences of the functional used for geometry optimizations. Due to the high computational cost of geometry optimizations and frequency calculations, in many (if not most) quantum chemical investigations of medium-sized and large systems these calculations are performed at the DFT level in conjunction with an economical basis set (normally of triple-zeta quality for medium-sized systems and double-zeta quality for large systems) and then the single-point energies are refined using a higher level of theory. This is also the case in economical composite ab initio procedures (e.g., W1, W2, W1-F12, W2-F12, ccCA, G4, G4(MP2), and CBS-QB3)[7,8,9,10] where the geometries and frequencies are calculated with the B3LYP functional in conjunction with a triple-zeta quality basis set and the energies are extrapolated to the CCSD(T)/CBS limit. While most composite ab initio methods by default use the B3LYP functional for the geometry and frequency calculations, it is worth re-examining this choice in the context of the large and diverse set of molecules in the W4-11-GEOM database. To do this, we use the DFT methods considered in the present work to generate reference geometries for W1-F12 theory. The resulting W1-F12 energies (using the various DFT reference geometries) were compared to W1-F12 energies obtained with the CCSD(T)/CBS reference geometries in the W4-11-GEOM database. The RMSDs in the

electronic energy due to the change in reference geometry are given in Table 5. Before proceeding to a discussion of the RMSDs in Table 5, we note that errors in the bond distances (whether they are overestimations or underestimations) should in principle lead to overestimation of the molecular energies relative to those obtained at the CCSD(T)/CBS equilibrium geometries. Indeed, the mean-signed-deviations for all the functionals are positive and essentially equal to the mean-absolute deviations (see Table 5).

Table 5. Effect of the choice of the DFT reference geometry on molecular energies calculated via W1-F12 theory for the 122 molecules in the W4-11-GEOM database (error statistics are in kJ mol^{-1}).[a,b,c,d]

		RMSD	MAD	MSD
GGA	B97-D	2.92	1.05	1.05
	HCTH407	2.53	0.60	0.59
	BLYP	2.49	1.75	1.75
	BP86	1.68	1.26	1.26
	BPW91	1.48	1.05	1.05
	PBE	1.48	1.09	1.09
	SOGGA11	0.61	0.43	0.42
	N12	0.53	0.39	0.37
MGGA	M11-L	3.36	2.53	2.52
	VSXC	2.62	0.58	0.58
	τ-HCTH	2.48	0.53	0.53
	M06-L	2.16	0.37	0.35
	TPSS	1.14	0.75	0.75
	MN15-L	0.85	0.61	0.60
	MN12-L	0.78	0.58	0.58
HGGA	BH&HLYP	1.72	1.24	1.23
	B97-1	0.55	0.24	0.23
	SOGGA11-X	0.54	0.29	0.29
	PBE0	0.40	0.25	0.25
	mPW1PBE	0.40	0.25	0.24
	mPW1PW91	0.39	0.24	0.24
	APF	0.33	0.21	0.21
	B3LYP	0.29	0.20	0.19
	B3P86	0.28	0.18	0.17
	mPW3PBE	0.28	0.19	0.18
	B3PW91	0.26	0.18	0.17
	mPW1LYP	0.25	0.18	0.17
	X3LYP	0.25	0.18	0.17
HMGGA	τ-HCTHh	2.31	0.42	0.41
	M06-HF	1.97	1.23	1.23

	BMK	1.39	0.46	0.45
	M08-HX	0.81	0.54	0.54
	M05-2X	0.77	0.44	0.43
	M05	0.69	0.33	0.33
	M06-2X	0.66	0.37	0.35
	M06	0.60	0.39	0.37
	MN15	0.57	0.32	0.31
	B1B95	0.46	0.30	0.29
	PW6B95	0.44	0.30	0.29
	TPSSh	0.36	0.21	0.21
RS	M11	0.81	0.57	0.57
	N12-SX	0.73	0.49	0.48
	ωB97	0.72	0.39	0.38
	MN12-SX	0.60	0.46	0.45
	ωB97-X	0.60	0.34	0.34
	CAM-B3LYP	0.49	0.32	0.31
	ωB97-XD	0.45	0.28	0.28
DH	MP2	1.51	0.58	0.57
	PBE0-DH	0.70	0.45	0.44
	PBEQI-DH	0.54	0.35	0.33
	B2-PLYP	0.22	0.10	0.09
	DSD-PBEP86	0.17	0.08	0.07
	B2GP-PLYP	0.11	0.06	0.04
	mPW2PLYP	0.10	0.06	0.04

[a]GGA = generalized gradient approximation, HGGA = hybrid-GGA, MGGA = meta-GGA, HMGGA = hybrid-meta-GGA, RS = range-separated, DH = double hybrid. [b]The reference values are CCSD(T)/CBS energies from W1-F12 theory calculated using the best CCSD(T)/CBS reference geometries in the W4-11-GEOM database. [c]DFT geometries are calculated in conjunction with the Def2-TZVPP basis set. [d]RMSD = root-mean-square deviation, MAD = mean-absolute deviation, MSD = mean-signed deviation.

Since CCSD(T)-based composite ab initio methods are capable of sub-kcal-per-mole accuracy for non-multireference species, we will deem errors arising from the reference geometry below 0.5 kJ mol^{-1} (i.e., ~12% of 1 kcal mol^{-1}) as acceptable. All the GGA methods result in large RMSDs ranging from 2.9 (B97-D) and 0.5 (N12) kJ mol^{-1}. In particular, the B97-D, HCTH407, BLYP, BP86, BPW91, and PBE methods result in RMSDs > 1 kJ mol^{-1} and are not recommended for geometry optimizations. Overall, the MGGA methods do not perform better than the GGA methods and result in large errors ranging from 3.4 (M11-L) and 0.8 (MN12-L) kJ mol^{-1}. Where M11-L, VSXC, τ-HCTH, and M06-L result in RMSDs > 2 kJ mol^{-1} and TPSS results in an RMSD > 1 kJ mol^{-1}. These MGGAs are thus not recommended for geometry optimizations.

Performance is substantially improved when moving to the HGGAs, this by itself is very much expected, however, the magnitude of the reductions in RMSDs across the board are somewhat surprising. The BH&HLYP functional is the main outlier here with a large RMSD of 1.7 kJ mol^{-1}. Apart of B97-1 and SOGGA11-X which result in RMSD ≈ 0.5 kJ mol^{-1}, all the HGGA methods result in excellent performance with RMSDs ≤ 0.5 kJ mol^{-1}. In particular, the six HGGA functionals (B3LYP, B3P86, mPW3PBE, B3PW91, mPW1LYP, and X3LYP) result in RMSDs between 0.25–0.30 kJ mol^{-1} and are all recommended for geometry optimizations. Notably, the best performing functionals include the popular B3LYP method, which confirms that this is a good method to use for geometry optimizations in composite ab initio procedures. However, of the recommended functionals, B3LYP is not the best performer, and methods such as B3PW91, mPW1LYP, and X3LYP have a slight advantage over B3LYP.

With the exception of TPSSh, B1B95, and PW6B95, all the HMGGA methods result in disappointing performance with RMSDs ranging from 2.3 (τ-HCTHh) and 0.6 (MN15) kJ mol^{-1}. In particular, τ-HCTHh, M06-HF, and BMK result in large RMSDs > 1.4 kJ mol^{-1} and are not recommended for geometry optimizations. The best performing HMGGAs result in RMSDs of 0.46 (TPSSh), 0.44 (B1B95), and 0.36 (PW6B95) kJ mol^{-1}. Nevertheless, these RMSDs are larger than those obtained by the best performing HGGAs (*vide supra*). In a similar manner, the range-separated procedures do not provide an improvement over the global hybrids for these systems. The best range-separated functionals (CAM-B3LYP and ωB97-XD) result in RMSDs of 0.49 and 0.45 kJ mol^{-1}, respectively.

A significant improvement in performance over the hybrid GGAs is provided by the double-hybrid methods. With the exception of PBE0-DH and PBEQI-DH, all the DHDFT methods result in excellent performance with RMSDs ranging between 0.22 (B2-PLYP) and 0.10 (mPW2PLYP) kJ mol^{-1}. In particular, B2GP-PLYP and mPW2PLYP give performance which is comparable to that of the CCSD(T)/CBS reference geometries.[89] It is important to

point out that with accelerating techniques such as density fitting (or resolution of the identity)[90,91] the MP2 step of the DHDFT calculation reaches only 25–30% of the total CPU time for medium-sized systems such as C_{60}.[89] Finally, in contrast to DHDFT, MP2 results in poor performance with an RMSD of 1.5 kJ mol^{-1} and is therefore not recommended for geometry optimizations.

Finally, it is of interest to examine the effect of using the same DFT functional for obtaining both the geometries and zero-point vibrational energies (ZPVEs). For this purpose, we consider the functionals for which optimal ZPVE scaling factors have been obtained in conjunction with the Def2-TZVPP basis set in ref. 92. Table S11 of the Supporting Information gives the RMSDs over the 122 ZPVE-inclusive W1-F12 energies in the W4-11-GEOM database. Overall, the RMSDs for the ZPVE-exclusive (Table 5) and ZPVE-inclusive (Table S11) energies differ by relatively small amounts of up to 0.5 kJ mol^{-1}.

4. Conclusions

We evaluate the performance of a variety of contemporary DFT methods for obtaining the structures of the 122 first- and second-row species in the W4-11-GEOM database, which includes a total of 246 unique bonds: 117 H–X, 65 X–Y, 49 X=Y, and 15 X≡Y bonds, and 133 key bond angles: 96 X-Y-H, 22 X-Y-Z, and 15 H-X-H angles. The reference structures in the W4-11-GEOM database are optimized at the CCSD(T)/jul-cc-pV(6+d)Z level of theory (or CCSD(T)/jul-cc-pV(5+d)Z for 14 larger systems). We evaluate the performance 52 DFT methods across the rungs of Jacob's Ladder in conjunction with the Def2-*n*ZVPP (*n* = T, Q), cc-pV(T+d)Z, and jul-cc-pV(T+d)Z basis sets. Our main conclusions can be summarized as follows:

- In terms of bond distances, the best performing functionals from each rung of Jacob's Ladder are, root-mean-square deviations (RMSDs) in parentheses: SOGGA11

(0.0086), τ-HCTH (0.0088), X3LYP (0.0058), TPSSh (0.0054), and DSD-PBEP86 0.0032 (Å).

- The best performing double-hybrid DFT methods, DSD-PBEP86, B2-PLYP, B2GP-PLYP, and mPW2-PLYP, achieve near-CCSD(T) accuracy with RMS deviations of 0.0032–0.0043 Å.
- For comparison, MP2 theory attains an overall RMSD of 0.0081 Å, where particularly poor performance is observed for double and triple bonds.
- The single X–Y bonds pose a particular challenge for many conventional DFT functionals. The best performing functionals from each rung of Jacob's Ladder are (RMSDs in parentheses): the GGAs SOGGA11 (0.0109) and HCTH407 (0.0112); MGGAs MN15-L (0.0086) and τ-HCTH (0.0099); HGGAs X3LYP (0.0070) and mPW1LYP (0.0070); HMGGAs TPSSh (0.0074) and τ-HCTH (0.0082); and DHDFT method DSD-PBEP86 (0.0037 Å).
- In terms of bond angles, most of the conventional DFT methods attain RMSDs ranging between 0.5–1.0°. The best performing HGGA and HMGGA methods (τ-HCTHh, B97-1, SOGGA11-X, and TPSSh) attain RMSDs between 0.4–0.5°. Most of the DHDFT methods result in excellent performance with RMSDs ranging between 0.25° (DSD-PBEP86) and 0.40° (mPW2-PLYP and PBEQI-DH). For comparison MP2 attains a substantially larger RMSD of 0.66°.
- With few exceptions, the conventional DFT methods exhibit a weak basis set dependency, such that the RMSDs of the Def2-TZVPP and Def2-QZVPP basis sets are smaller than 0.0001 Å. In a similar manner, the Def2-TZVPP, cc-pV(T+d)Z, and jul-cc-pV(T+d)Z basis sets show similar performance.
- Finally, we examine the effect of the reference DFT geometry on the final energy in the context of economical composite ab initio methods. Most GGA and MGGA methods

result in large RMSDs of up to 3.4 kJ mol^{-1} in the final W1-F12 energies and are thus not recommended for geometry optimizations in composite ab initio procedures. Performance is substantially improved when moving to the HGGAs, where six functionals (i.e., B3LYP, B3P86, mPW3PBE, B3PW91, mPW1LYP, and X3LYP) result in RMSDs between 0.25–0.30 kJ mol^{-1} and are thus recommended for geometry optimizations. Interestingly, HMGGA methods do not offer an improvement over the HGGA methods. A significant improvement in performance over the hybrid GGAs is provided by the double-hybrid methods. In particular, B2GP-PLYP and mPW2PLYP give performance which is comparable to that of the CCSD(T)/CBS reference geometries with RMSDs of merely 0.11 and 0.10 kJ mol^{-1}, respectively.

■ ACKNOWLEDGMENTS

We gratefully acknowledge the generous allocation of computing time from the National Computational Infrastructure (NCI) National Facility, and system administration support provided by the Faculty of Science at UWA to the Linux cluster of the Karton group. AK is the recipient of an Australian Research Council (ARC) Future Fellowship (Project No. FT170100373).

■ SUPPORTING INFORMATION

Overview of the 122 molecules in the W4-11-GEOM database (Table S1); Overview of the performance of DFT procedures with the Def2-TZVPP basis set for the 246 bonds in the W4-11-GEOM database and subsets thereof (Table S2); Reference CCSD(T)/CBS bond distances in the W4-11-GEOM database (Table S3); Effect of D3BJ dispersion corrections on the performance of selected DFT methods (Table S4); Overview of the performance of DFT procedures for X–H (Table S5), X–Y (Table S6), X=Y (Table S7) bonds; Reference

CCSD(T)/CBS bond angles in the W4-11-GEOM database (Table S8); Overview of the performance of DFT procedures with the Def2-QZVPP (Table S9) and cc-pV(T+d)Z and jul-cc-pV(T+d)Z (Table S10) basis sets; Effect of the choice of the DFT reference geometry on ZPVE-inclusive W1-F12 energies (Table S11); Error statistics for bond angles in the W4-11-GEOM database (Table S12); CCSD(T)/CBS reference geometries for all structures in the W4-11-GEOM database (Table S13); Absolute W1-F12 energies calculated using of the CCSD(T)/CBS and DFT reference geometries (Table S14).

■ REFERENCES

[1] A. Domenicano, I. Hargittai, Eds. Accurate molecular structures. Their determination and importance; Oxford University Press: New York, 1992.

[2] J. Demaison, J. Boggs, A. Császár, Eds. Equilibrium molecular structures: from spectroscopy to quantum chemistry; CRC Press: Boca Raton, FL, 2011.

[3] H. B. Schlegel, WIREs Comput. Mol. Sci. 2011, 1, 790.

[4] A. D. Becke, J. Chem. Phys. 1993, 98, 5648.

[5] J. M. L. Martin, S. Parthiban, W1 and W2 theory and their variants: thermochemistry in the kJ/mol accuracy range. Understanding Chemical Reactivity, Vol. 22: Quantum-Mechanical Prediction of Thermochemical Data, J. Cioslowski, ed. (Kluwer, Dordrecht, 2001), pp. 31–65.

[6] A. Karton, J. M. L. Martin, J Chem Phys, 2012, 136, 124114.

[7] A. Karton, WIREs Comput. Mol. Sci. 2016, 6, 292.

[8] N. DeYonker, T. R. Cundari, A. K. Wilson, in: Piecuch P, Maruani J, Delgado-Barrio G, Wilson S (Eds.), Advances in the Theory of Atomic and Molecular Systems (Progress in Theoretical Chemistry and Physics, Vol. 19), Springer Netherlands, Dordrecht, 2009 pp. 197–224.

[9] L. A. Curtiss, P. C. Redfern, K. Raghavachari, WIREs Comput Mol Sci, 2011, 1, 810.

[10] J. A. Montgomery Jr., M. J. Frisch, J. W. Ochterski, G. A. Petersson, J. Chem. Phys. 1999, 110, 2822.

[11] A. D. Boese, J. M. L. Martin, J. Chem. Phys. 2004, 121, 3405.

[12] B. Chan, J. Deng, L. Radom, J. Chem. Theory Comput. 2011, 7, 112.

[13] A. E. Mattsson, Science 2002, 298, 759.

[14] R. Peverati, D. G. Truhlar, Philos. Trans. R. Soc. A 2014, 372, 20120476.

[15] P. Morgante, R. Peverati, Int. J. Quantum Chem. 2020, 120, e26332.

[16] P. Verma, D. G. Truhlar, Trends Chem. 2020, 2, 302.

[17] L. Goerigk, N. Mehta, Aust. J. Chem. 2019, 72, 563.

[18] N. Mardirossian, M. Head-Gordon, Mol. Phys. 2017, 115, 2315.

[19] L. Goerigk, A. Hansen, C. A. Bauer, S. Ehrlich, A. Najibi, S. Grimme, Phys. Chem. Chem. Phys. 2017, 19, 32184.

[20] L. Goerigk, S. Grimme, Phys. Chem. Chem. Phys. 2011, 13, 6670.

[21] É. Brémond, M. Savarese, N. Q. Su, Á. J. Pérez-Jiménez, X. Xu, J. C. Sancho-Garca, C. Adamo, J. Chem. Theory Comput. 2016, 12, 459.

[22] M. Piccardo, E. Penocchio, C. Puzzarini, M. Biczysko, V. Barone, J. Phys. Chem. A 2015, 119, 2058.

[23] E. Penocchio, M. Piccardo, V. Barone, J. Chem. Theory Comput. 2015, 11, 4689.

[24] P. Morgante, R. Peverati, Chem. Phys. Lett. 2021, 765, 138281.

[25] K. L. Bak, J. Gauss, P. Jørgensen, J. Olsen, T. Helgaker, J. F. Stanton, J. Chem. Phys. 2001, 114, 6548.

[26] P. R. Spackman, D. Jayatilaka, A. Karton, J. Chem. Phys. 2016, 145, 104101.

[27] A. Karton, S. Daon, J. M. L. Martin, Chem. Phys. Lett. 2011, 510, 165.

[28] C. Lee, W. Yang, R. G. Parr, Phys. Rev. B 1988, 37, 785.

[29] A. D. Becke, Phys. Rev. A 1988, 38, 3098.

[30] S. Grimme, J. Comput. Chem. 2006, 27, 1787.

[31] A. D. Boese, N. C. Handy, J. Chem. Phys. 2001, 114, 5497.

[32] J. P. Perdew, K. Burke, M. Ernzerhof, Phys. Rev. Lett. 1996, 77, 3865.

[33] J. P. Perdew, Phys. Rev. B 1986, 33, 8822.

[34] J. P. Perdew, J. A. Chevary, S. H. Vosko, K. A. Jackson, M. R. Pederson, D. J. Singh, C. Fiolhais, Phys. Rev. B 1992, 46, 6671.

[35] R. Peverati, Y. Zhao, D. G. Truhlar, J. Phys. Chem. Lett. 2011, 2, 1991.

[36] R. Peverati, D. G. Truhlar, J. Chem. Theory Comput. 2012, 8, 2310.

[37] Y. Zhao, D. G. Truhlar, J. Chem. Phys. 2006, 125, 194101.

[38] J. M. Tao, J. P. Perdew, V. N. Staroverov, G. E. Scuseria, Phys. Rev. Lett. 91, 2003, 146401.

[39] A. D. Boese, N. C. Handy, J. Chem. Phys. 2002, 116, 9559.

[40] T. van Voorhis, G. E. Scuseria, J. Chem. Phys. 1998, 109, 400.

[41] R. Peverati, D. G. Truhlar, J. Phys. Chem. Lett. 2012, 3, 117.

[42] R. Peverati, D. G. Truhlar, Phys. Chem. Chem. Phys. 2012, 10, 13171.

[43] H. S. Yu, X. He, S. L. Li, D. G. Truhlar, Chem. Sci. 2016, 7, 5032.

[44] A. D. Becke, J. Chem. Phys. 1993, 98, 1372.

[45] A. D. Becke, J. Chem. Phys. 1993, 98, 5648.

[46] P. J. Stephens, F. J. Devlin, C. F. Chabalowski, M. J. Frisch, J. Phys. Chem. 1994, 98, 11623.

[47] C. Adamo, V. Barone, J. Chem. Phys. 1999, 110, 6158.

[48] F. A. Hamprecht, A. J. Cohen, D. J. Tozer, N. C. Handy, J. Chem. Phys. 1998, 109, 6264.

[49] X. Xu, Q. Zhang, R. P. Muller, W. A. Goddard, J. Chem. Phys. 2005, 122, 014105.

[50] R. Peverati, D. G. Truhlar, J. Chem. Phys. 2011, 135, 191102.

[51] A. Austin, G. Petersson, M. J. Frisch, F. J. Dobek, G. Scalmani, K. Throssell, J. Chem. Theory Comput. 2012, 8, 4989.

[52] C. Adamo, V. Barone, J. Chem. Phys. 1998, 108, 664.

[53] J.-D. Chai, M. Head-Gordon, J. Chem. Phys. 2008, 084106, 128.

[54] R. Peverati, D. G. Truhlar, Phys. Chem. Chem. Phys. 2012, 14, 16187.

[55] T. Yanai, D. Tew, N. C. Handy, Chem. Phys. Lett. 2004, 393, 51.

[56] Y. Zhao, N. E. Schultz, D. G. Truhlar, J. Chem. Phys. 2005, 123, 161103.

[57] Y. Zhao, N. E. Schultz, D. G. Truhlar, J. Chem. Theory Comput. 2006, 2, 364.

[58] Y. Zhao, D. G. Truhlar, Theor. Chem. Acc. 2008, 120, 215.

[59] Y. Zhao, D. G. Truhlar, J. Chem. Theory Comput. 2008, 4, 1849.

[60] A. D. Boese, J. M. L. Martin, J. Chem. Phys. 2004, 121, 3405.

[61] A. D. Becke, J. Chem. Phys. 1996, 104, 1040.

[62] V. N. Staroverov, G. E. Scuseria, J. Tao, J. P. Perdew, J. Chem. Phys. 2003, 119, 12129.

[63] Y. Zhao, D. G. Truhlar, J. Phys. Chem. A 2005, 109, 5656.

[64] R. Peverati, D. G. Truhlar, J. Phys. Chem. Lett. 2011, 2, 2810.

[65] S. Grimme, J. Chem. Phys. 2006, 124, 034108.

[66] T. Schwabe, S. Grimme, Phys. Chem. Chem. Phys. 2006, 8, 4398.

[67] A. Karton, A. Tarnopolsky, J.–F. Lamere, G. C. Schatz, J. M. L. Martin, J. Phys. Chem. A 2008, 112, 12868.

[68] S. Kozuch, J. M. L. Martin, J. Comput. Chem. 2013, 34, 2327.

[69] S. Kozuch, J. M. L. Martin, Phys. Chem. Chem. Phys. 2011, 13, 20104.

[70] É. Brémond, C. Adamo, J. Chem. Phys. 2011, 135, 024106.

[71] É. Brémond, J. C. Sancho-García, Á. J. Pérez-Jiménez, C. Adamo, J. Chem. Phys. 2014, 141, 031101.

[72] F. Weigend, R. Ahlrichs, Phys. Chem. Chem. Phys. 2005, 7, 3297.

[73] T. H. Dunning, J. Chem. Phys. 1989, 90, 1007.

[74] R. A. Kendall, T. H. Dunning, R. J. Harrison, J. Chem. Phys. 1992, 96, 6796.

[75] K. A. Peterson, T. H. Dunning, J. Chem. Phys. 2002, 117, 10548.

[76] E. Papajak, D. G. Truhlar, J. Chem. Theory Comput. 2011, 7, 10.

[77] H.-J. Werner, P. J. Knowles, G. Knizia, F. R. Manby, M. Schutz, P. Celani, T. Korona, R. Lindh, A. Mitrushenkov, G. Rauhut, et al. MOLPRO (version 2012.1) is a package of ab initio programs. Available at: http://www.molpro.net.

[78] H.-J. Werner, P. J. Knowles, G. Knizia, F. R. Manby, M. Schutz, WIREs Comput. Mol. Sci. 2012, 2, 242.

[79] M. J. Frisch, G. W. Trucks, H. B. Schlegel, G. E. Scuseria, M. A. Robb, J. R. Cheeseman, G. Scalmani, V. Barone, G. A. Petersson, H. Nakatsuji, et al. Gaussian 16, Revision A.03; Gaussian, Inc., Wallingford, CT, 2016.

[80] G. Vacek, J. M. Galbraith, Y. Yamaguchi, H. F. Schaefer, R. H. Nobes, A. P. Scott, L. Radom, J. Phys. Chem. 1994, 98, 8660.

[81] P. J. Wilson, D. J. Tozer, Chem. Phys. Lett. 2002, 352, 540.

[82] R. C. Mawhinney, J. D. Goddard, J. Mol. Struct.: THEOCHEM 2003, 629, 263.

[83] S. Grimme, WIREs Comput. Mol. Sci. 2011, 1, 211.

[84] S. Grimme, J. Antony, S. Ehrlich, H. Krieg, J. Chem. Phys. 2010, 132, 154104.

[85] S. Grimme, S. Ehrlich, L. Goerigk, J. Comput. Chem. 2011, 32, 1456.

[86] A. D. Becke, E. R. Johnson, J. Chem. Phys. 2005, 123, 154101.

[87] N. Mardirossian and M. Head-Gordon, J. Chem. Theory Comput. 2013, 9, 4453.

[88] L.-J. Yu, F. Sarrami, A. Karton, R. J. O'Reilly. Mol. Phys. 2015, 113, 1284.

[89] J. M. L. Martin, G. Santra, *Isr. J. Chem.* 2020, 60, 787.

[90] R. A. Kendall, H. A. Früchtl, *Theor. Chem. Acc.* 1997, 97, 158.

[91] F. Weigend, M. Häser, H. Patzelt, R. Ahlrichs, *Chem. Phys. Lett.* 1998, 294, 143.

[92] M. K. Kesharwani, B. Brauer, J. M. L. Martin, *J. Phys. Chem. A* 2015, 119, 1701.